ORIGINAL ARTICLE

Taylor&Francis healthsciences

Extracranial Stereotactic Radioablation

Physical Principles

Lech Papież, Robert Timmerman, Colleen DesRosiers and Marcus Randall

From the Department of Radiation Oncology, Indiana University School of Medicine, Indianapolis, USA

Correspondence to: Lech Papież, Department of Radiation Oncology, Indiana University School of Medicine, 535 Barnhill Drive, Indianapolis, IN 46202, USA. E-mail: lpapiez@iupui.edu

Acta Oncologica Vol. 42, No. 8, pp. 882–894, 2003

Extracranial stereotactic radioablation (ESR) involves treating well-demarcated targeted tissues (e.g. tumor with minimal margin for set-up uncertainties) with very large doses of radiation in single or a few fractions with the intent of causing profound late tissue damage within the targeted volume. In such circumstances, considerable effort must be taken to reduce non-target tissue exposure to the high dose levels in order to prevent late complications to involved organs. Consequently, the following conditions for effective delivery of the ESR techniques have to be satisfied: 1) delivery of a high dose per fraction, i.e. 10–24 Gy; 2) delivery of only a few fractions per course of treatment (e.g. 1–4); 3) shaping of the prescription isodose surface conformally to the target surface; 4) delivery of a non-uniform dose distribution within the target with the highest dose in centrally located regions of hypoxia; 5) rapid fall-off of dose from the target volume to healthy tissue in all directions. In this paper it is shown that high doses per fraction in few fractions can be delivered to a variety of locations with both efficacy and acceptable toxicity (conditions 1 and 2). Conformal shaping of the high isodose surfaces is best accomplished by employing many beams (5–10) each with carefully milled apertures precisely coincident with the target projection (condition 3). Beam intensity modulation creating parabolic beam entrance fluence profiles both concentrates the highest dose in central regions of tumor hypoxia and increases fall-off gradients outside of the target (conditions 4 and 5). It is also shown that isotropic, highly non-coplanar beam arrangements avoiding oppositional fields allow more optimal fall-off gradients to normal tissue as opposed to coplanar treatments (condition 5).

Received 22 November 2002
Accepted 4 June 2003

The established success of stereotactic radiosurgery in treating both benign and malignant tumors within and around the cranial compartment has logically led to attempts to mimic these treatments within other body regions. A particular realization of the idea of treating extracranial targets in a manner similar to stereotactic radiosurgery has been accomplished through the utilization of the device called the Stereotactic Body Frame (SBF, Elekta Oncology) (1–3). The SBF can be utilized for treatment of tumors located in the torso of the body. Typical organs that can be treated are lung and liver, though treatment of other areas in the abdomen and pelvis can also be targeted. Other treatments than SBF-based techniques are also applied in extracranial stereotactic radiosurgery but those usually require specialized equipment, e.g. Cyber Knife or Novalis treatment units and image-guided delivery technology (4, 5).

The design and parameters of the SBF have been described in detail in (1). The SBF combines a reliable immobilization system, a device capable of decreasing internal organ motion and an array of fiducial marks and measuring tools. As a result, the SBF facilitates accurate patient positioning as well as precise targeting of tumors based on assigned Cartesian coordinates throughout the body. With this technique, the isocenter of the target is identified based on coordinates rather than patient's skin and bony landmarks. Appropriate implementation of this technique results in a significant change in treatment routine compared to conventional therapy, potentially improving control within the target. Researchers from the Karolinska Hospital accumulated considerable clinical experience validating their approach to utilization of the SBF (1–3). Given this experience it seemed reasonable for us to follow the general recommendations of the Karolinska group when we started to utilize SBF for radiotherapy treatments in early 1997. With time, however, modifications of some aspects of the original Karolinska approach were introduced when we believed that dose distributions, or dose delivery processes, could be further refined.

The purpose of this paper is to discuss general principles of shaping dose distributions for extracranial stereotactic radioablation (ESR). In particular, we investigate parameters of the *isotropicity* of the dose distribution in regions adjacent to the target and the *gradient* of the dose decrease

 ISSN 0284-186X
DOI: 10.1080/02841860310013490

away from the tumor boundary. These are crucial factors for ESR. As this technique is characterized by high dose per fraction, the minimization of the damage to healthy tissue within the organ where the tumor is located is paramount for the success of the method. Since irradiation to high dose levels to organs such as lung or liver, where ESR-treated tumors are situated, cannot be avoided, the primary incentive is to minimize the volume outside of the target that is exposed to high dose. This requirement nearly always comes at the cost of exposing larger patient volumes to relatively low doses. However, these lower dose values usually do not lead to unacceptable levels of toxicity.

The rapid fall-off of dose from the tumor in all directions can be achieved by the convergence of multiple non-coplanar beams on the target from directions as isotropically distributed in space as is clinically feasible. To establish these general principles, we consider generic situations of variable symmetry ranging from purely axial irradiations (coplanar, rotational treatments) to ideally isotropic irradiations. The goal is to find exact, analytic formulas representing dose distributions for cases of variable isotropicity of beam arrangements. Formulas of this kind allow an understanding of qualitative and quantitative properties of ESR dosimetry that cannot always be inferred from numerical computations derived by radiotherapy planning systems designed for individual computation of each specific case.

As part of our experience with the SBF at Indiana University, we have been conducting trials assessing the effect of dose escalation on toxicity. We have confirmed the feasibility of treatments using dose prescriptions that we elaborate on in this paper. Results of phase I dose escalation study reached dose levels of 24 Gy $\times$ 3 fractions (6). The biological effective dose of these extracranial treatments exceeds that used for stereotactic radiosurgery within serially functioning tissues of the brain. Thus these treatments have ablative characteristics and are biologically different from conventionally fractionated therapy. Their radiobiological rationale, as well as the context of their clinical applications, is discussed in more detail in separate publications (6, 7).

1. MATERIALS AND METHODS

Objectives

As discussed above, ESR involves delivering focused, very high-dose radiation per fraction treatment characterized by isotropic and rapid dose fall-off to normal surrounding tissues. This type of 'imitation' of Gamma Knife treatments by linear accelerator configurations is possible though generally not practiced in radiation therapy. The proof that any Gamma Knife treatment may be reproduced by linear accelerator based, intensity-modulated irradiations has been previously described in (8). While the publication (8) dealt mainly with general aspects of the equivalence between multiple shots Gamma Knife treatments and isocentric, intensity-modulated therapies, this presentation, in contrast, concentrates on clinically feasible realizations of linear accelerator treatments that imitate Gamma Knife therapies in some approximation only.

To imitate properties of Gamma Knife treatments for ECSR therapy specific requirements need to be satisfied. These are:

i) The shape of the iso-surface defined by the dose prescribed conforms to the outline of the target and highest doses delivered outside of the tumor are confined to regions that spread uniformly on the outer boundary of the targeted volume.
ii) Rapid fall-off of dose from the tumor volume to healthy tissue isotropically in all directions.
iii) Non-uniform dose distribution throughout the volume of the tumor, with the highest dose delivered to the central portion of the tumor where hypoxic cells potentially reside.
iv) Delivery of high dose per fraction to the tumor volume (of the order of 10 to 20 Gy).
v) A small number of fractions per course of treatment (e.g. 1–4).

Conditions (i) and (ii) require that a relatively large number of non-coplanar beams be utilized for ESR treatments. Conditions (i), (ii) and (iii) are achieved for ESR treatments in a somewhat different manner than that for Gamma Knife therapy. Instead of combining multiple shots with various weighting factors, these distributions can be realized by appropriate shaping of intensities of a limited number of non-coplanar beams. That these two approaches can lead to equivalent results has been discussed in detail in the past (8). In particular, formulas that interrelate beam intensities of modulated linear accelerator therapy with weighting factors of equivalent Gamma Knife therapy have been provided in (8). Conditions (iv) and (v) are rationalized in previous publications (6, 7). Their clinical validation is already well established and is a result of ESR fractionation experience accumulated by the Karolinska Hospital and by our institution.

Rapid dose fall-off and the spatial distribution of beam directions

The rapid fall-off of dose from the tumor in all directions can be achieved with multiple non-coplanar beams converging on the target volume from directions that are as isotropically distributed in space as possible. To establish this general principle we consider generic situations of variable symmetry ranging from purely axial irradiations (planar treatments) to ideally isotropic irradiations. The goal of these considerations is to find basic, analytic

formulas representing dose distributions for cases of variable isotropicity of beam arrangements. This is in contrast to standard approaches based on computer algorithm calculations, which by nature provide only partial information for such comparisons because they have to rely on particular numerical evaluations. The approach based on analytic solutions has to be inherently simplified to admit the appropriate, closed form of solution to the problem under consideration. Still, even for simplified models, there are only a few cases where such solutions are possible. A few explicit examples of such calculations have been provided elsewhere (9–13) and few more we derive below.

Let us start with the description of the geometry of irradiations in the general case. The unit radius sphere S drawn in Fig. 1 (with the center placed at the origin O of the system of Cartesian coordinates) represents a tumor. A cylinder C tangential to this sphere represents geometrically a beam irradiating the tumor. We assume that the beam consists of rays parallel to the central axis of a cylinder along which all irradiating particles move towards the spherical tumor. Moreover, rays are assumed to be uniformly distributed throughout the unit radius circle $D = \{(x, y) \in P_{\perp C},\ x^2+y^2 \le 1\}$ that forms the base of the cylinder C, i.e. the intensity P_{uni} of the beam (defined on the circle D formed by a section of the cylinder C by a plane $P_{\perp C}$ perpendicular to its axis) is a constant that, for the sake of simplicity, may be assumed to be equal to 1. Thus

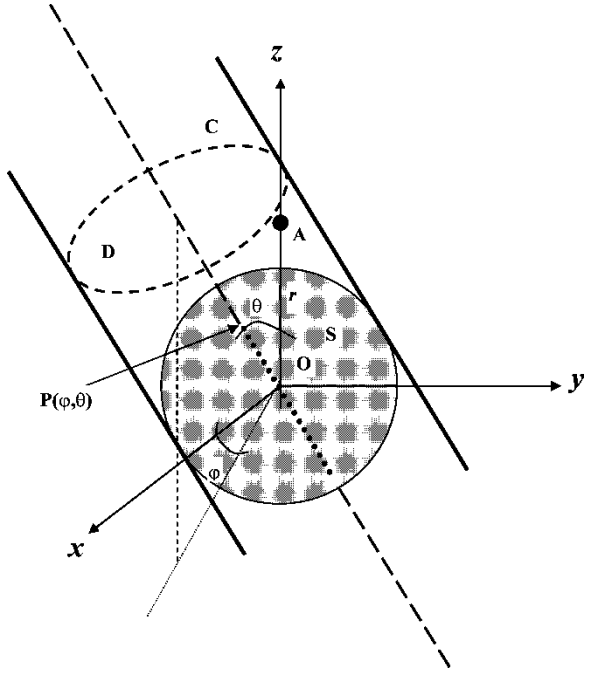

Fig. 1. Sphere S represents a tumor irradiated by cylindrical beam C with base D. The central axis of the cylinder C passes through the center of the sphere O and crosses the surface of the sphere at point $P(\varphi, \theta)$, where φ and θ denote angular parameters of the point $P \in S$. Point A is located outside the sphere S at distance r from its center along the z-axis.

$$P_{uni}(x,\ y) = \begin{cases} 1 & \text{for} \quad x^2+y^2 \le 1 \\ 0 & \text{for} \quad x^2+y^2 > 1 \end{cases} \qquad [1.1]$$

The direction of any cylindrical beam can be defined by a point $P(\varphi, \theta)$ on the unit sphere S where φ and θ denote angular coordinates of a point $P(\varphi, \theta)$ in a spherical system of coordinates (with radial coordinate being equal to 1 on unit sphere S). An arbitrary point A can be chosen in the xz plane located at a distance $r = \sqrt{x^2+z^2} \ge 1$ from the origin O. In particular this point can be located on z axis as illustrated in Fig. 1. The dose to point A can be determined relative to the dose at the tumor isocenter (i.e. at the origin point O) when multiple cylindrical beams, with various sets of angular parameters φ and θ, are configured. Three characteristic beam configurations that consist of highly symmetrical arrangements of multiple beams can be distinguished. First, one (A1) of these arrangements simulates the uniform coplanar irradiation, the second one, (A2), simulates a uniform, isotropic treatment and the third one, (A3), simulates irradiation as isotropic as possible, or practical, in a clinic. The first case (A1) of coplanar, uniform arc irradiation (i.e. standard 360° gantry arc rotation therapy) is modeled by a collection of beams with central axes distributed uniformly along the unit radius circle K in xz plane (Fig. 1). The circle K can be defined as a collection of points $P(\varphi, \theta)$ such that $K = \{P(\varphi, \theta)$: $\varphi = 0$ and $\varphi = \pi$, $\theta \in [0, \pi)\}$ where φ is the azimuthal angle in xy plane and θ is a polar angle between point of interest and z-axis. The second case (A2) of a uniform, isotropic irradiation is modeled by a collection of multiple beams the central axes of which uniformly scan the entire unit sphere $S = \{P(\varphi, \theta)$: $\varphi \in [0, 2\pi)$, $\theta \in [0, \pi)\}$. Finally, the third arrangement (A3) of clinically feasible, isotropic irradiation is modeled by a collection of multiple beams the central axes of which uniformly scan the subset PS of the unit sphere S given as

$$PS = \{P(\varphi',\ \theta')\text{:}\ \varphi' \in [0,\ 2\pi),\ \ \theta' \in [0,\ \pi/4) \quad \text{and} \quad \theta' \in [3\pi/4,\ \pi)\} \qquad [1.2]$$

where φ' is the azimuthal angle in xz plane and θ' is a polar angle between point of interest and y-axis.

When calculating the dose to a point A from a beam at a given fixed direction, we may assume in the first order approximation that the dose at A is proportional to the beam fluence at this point. In the case of beams with uniformly distributed rays, a fluence at A can acquire only two values depending on the orientation of the beam. If point A is inside the cylindrical volume for a particular orientation of the beam's central axis, then the fluence at A has a given, constant positive value (say 1, pending the relevant normalization). If, on the other hand, a point A is outside of the cylindrical volume for the beam's particular orientation, then the fluence at A is equal to 0. Thus the fluence $f(A)$ at A for any given irradiation IR is a characteristic function χ^A defined over the set of points

$P(\varphi, \theta)$ of the unit sphere S as

$$f^{A}_{(\varphi,\ \theta)} = \chi^{A}_{\beta}(\varphi,\ \theta) = \begin{cases} 1 & \text{if } P(\varphi,\ \theta) \in \beta \\ 0 & \text{otherwise} \end{cases} \qquad [1.3]$$

In the formula above the subset β of sphere S consists of points $P(\varphi, \theta)$ on a unit sphere S where central axes of all cylindrical beams containing point A cross the unit sphere S. Thus for the uniform, coplanar irradiation the subset β is a union of two arcs of the circle K for which $\varphi = 0,\ \theta \leq \arcsin(1/r)$ and $\pi - \theta \leq \arcsin(1/r)$, and for the non-coplanar, uniform isotropic irradiation the subset β is a union of two polar regions of the unit sphere S for which $\varphi \in [0,\ 2\pi),\ \theta \leq \arcsin(1/r)$ and $\pi - \theta \leq \arcsin(1/r)$, respectively. Consequently, the dose to point A from all beams that define a given irradiation IR equals, in the first order approximation, to a weighted sum $\Sigma_i\ \chi^{A}_{i}\omega_i$ of fluences at point A (provided the relevant normalization is applied) from each beam i. As a result, the following dose properties can be observed (see Appendix A for explicit calculations) for coplanar (A1), isotropically non-coplanar (A2) and clinically feasible, non-coplanar irradiation (A3).

i) For uniform, rotational, coplanar irradiation of a spherical tumor S with cylindrical beams C of constant intensity P_{uni} given as [1.1] the dose $D^{xz}_{A1}(r)$ to point A in xz plane at distance r from the point of origin O is given as [4.1] and dose $D^{y}_{A1}(r)$ to point A along the y-axis (perpendicular to axial xz plane and crossing origin O) is given as [4.2].
ii) For isotropic rotational, non-coplanar irradiation of a spherical tumor S with cylindrical beams C of constant intensity P_{uni} given as [1.1] the dose $D_{A2}(r)$ to point A along any radial direction at distance r from the point of origin O is given as [4.3].
iii) For clinically feasible, isotropic, non-coplanar irradiation of a spherical tumor S with cylindrical beams C of constant intensity P_{uni} given as [1.1] the dose $D^{xz}_{A3}(r)$ to point A in xz axial plane at distance r from the point of origin O is given as [4.4] and the dose $D^{y}_{A3}(r)$ to point A at distance r from O along the y-axis (perpendicular to axial xz plane and crossing origin O) is given as [4.5].

Graphs of two dimensional functions $D^{xz}_{A1}(r)$ [4.1], $D^{y}_{A1}(r)$ [4.2] , $D_{A2}(r)$ [4.3], $D^{xz}_{A3}(r)$ [4.4] and $D^{y}_{A3}(r)$ [4.4] are explicitly displayed in Fig. 2a. It is worth noticing that in the case of an isotropic, non-coplanar irradiation (A2) dose distribution $D_{A2}(r)$ [4.3] is characterized by spherical symmetry, i.e. the dose to point A depends only on the distance of point A from the origin O no matter in what direction this point is located relative to axes of the Cartesian system of coordinates. The situation is somewhat different for uniform, coplanar irradiation (A1) as well as for clinically feasible, isotropic, non-coplanar irradiation (A3). In both these cases, (Al) and (A3), the resulting dose distributions *are not* spherically symmetric. Instead, these distributions, as functions specified over 3-dimensional space, are invariant only with respect to rotations around the y-axis. Therefore, formulas $D^{xz}_{A1}(r)$ [4.1] and $D^{xz}_{A3}(r)$ [4.4] express the fact that these dose distributions in the xz plane have rotational symmetry and also give explicit dependence of dose as a function of distance from the center of the sphere S. For points that stay at a fixed distance r (for $r > 1$) from the origin O while moving away from plane xz the dose decreases for uniform, coplanar irradiation (Al) as well as for clinically feasible isotropic, non-coplanar irradiation (A3). This behavior of dose distributions is a consequence of a decreasing number of beams that contain point A when this point moves along a circle away from plane xz. In particular, for any point at distance $r > 1$ on the y-axis, the value of the dose is just equal to zero for (A1) irradiation as in this case $\mu(\beta) = 0$ when the beams' axes are outside of circle K. However, since for ESR we are primarily concerned with high doses to healthy tissue ($r > 1$), it is most relevant to compare doses in these regions of healthy tissue where dose values are largest. For cases under consideration these regions consist of points A ($r > 1$) located on the xy plane where dose is determined by formulas for $D^{xz}_{A1}(r)$ [4.1] , $D_{A2}(r)$ [4.3] and $D^{xz}_{A3}(r)$ [4.4]. Their behavior is also illustrated in Fig. 2a.

Notice that $D^{xz}_{A1}(r)$ [4.1] is a familiar formula of Cormack (9). This is one of few earlier known results that give analytic representation of dose distribution in radiation therapy. Originally, this result was derived using a rather involved method based on Radon transforms for circles in plane (9). The derivation in this paper is based on more heuristic arguments. However, in contrast to the Radon transform method, the derivation presented above is applicable to problems of 3-dimensional ($3D$) geometry. This allows us to obtain the equivalent of the Cormack result for $3D$ space given as [4.3] and [4.4]. The value of analytic formulas like [4.1], [4.3] and [4.4] is that they provide mathematically unambiguous demonstration of general properties of dose distributions. For example, in the early days of dose-planning optimization, Cormack's result [4.1] demonstrated how much the dose distributions determined by inverse dose calculations differed from required, ideal dose distributions (100% dose to target 0% to the rest of the body) when non-physical, negative beam intensities were cut from inverse solutions. Similarly, results [4.1], [4.3] and [4.4] demonstrate clearly (see Fig. 2a) the typical difference in dose gradients outside the tumor volume between coplanar and non-coplanar rotational irradiation techniques. In this comparison the non-coplanar irradiations (A2) and (A3) show a definite advantage of more favorable dose distributions in the proximity of the target. The highest doses for irradiations (A2) and (A3) are concentrated in regions directly adjacent to the tumor volume and they are more uniformly decreasing in all

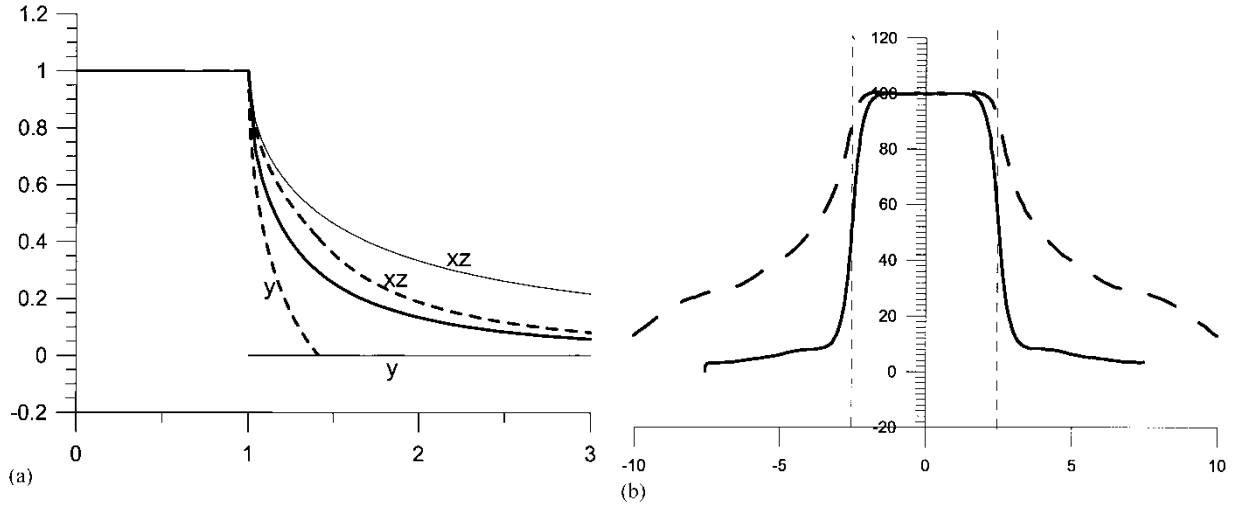

Fig. 2. (a) Dose distributions for irradiations (A1) – continuous thin line, (A2) – continuous thick line and (A3) – dashed line with beams of uniform intensity. The horizontal axis displays the distance from the center O of the tumor to point A where dose is specified, and the vertical axis shows the (normalized) dose delivered to point A. Markings xz and y displayed at given lines indicate that doses described by these lines are determined in the xz plane or along the y-axis. Notice the decreasing discrepancy between doses in the xz plane and along the y-axis with changing character of beam arrangements from purely coplanar (A1) to non-coplanar, isotropic (A2) (where this discrepancy vanishes completely). (b) Render Plan-generated dose distributions for rotational irradiation of the type (A1) i.e. full rotational therapy of a cylinder phantom of radius 10 (cm) executed with clinical, flat beams (Siemens KD2) of size 5 cm × 5 cm. The horizontal axis displays the distance from the center O of the spherical tumor to point A (see Fig. 1) where dose is specified, and the vertical axis shows the (normalized, in percent) dose delivered to point A. Profiles for the x-axis and z-axis are identical and are represented by the dashed line while a considerably less spread profile for the y-axis is represented by the continuous line (convention used is the same as that in Figs. 1 and 2a. Vertical dashed lines specify the size of the target (2.5 cm radius over each, x-, y- and z-axes) and indicate that the edge of the target is coincident with 50% isodose for the y-axis (inf–sup direction; perpendicular to the plane of beam rotation) and is coincident with 95% isodose for the x- and z-axes (both in plane of beam rotation). Notice the similarity (up to a smoothing property of real beam dose distribution) between dose profiles generated from planning system for real, clinical beams and from theoretical calculations (graphs based on analytic formulas) displayed in Fig. 2a.

directions away from the target than is the case for coplanar irradiation (A1). These properties of dose distributions for irradiations (A2) and (A3) have at least two clinical advantages over distribution [4.1] produced by uniform coplanar irradiation (A1). The first advantage emerges from the fact that relatively high doses of radiation are delivered for irradiations (A2) and (A3) to *all* areas adjacent to the tumor, whereas such doses are delivered to *some* areas only that are adjacent to the tumor for irradiation (A1). This advantage is clearly perceptible in situations when lack of proper recognition of the target (e.g. problem of micro-extensions (14) takes place or when unfortunate circumstances lead to doses not being delivered exactly as planned (larger than expected motion of the target or error in patient setup). Then the relatively high doses of radiation delivered for arrangements (A2) and (A3) to *all* areas adjacent to the tumor have a much better chance of correcting the unintended errors in radiotherapy tumor targeting. In cases that are not so isolated, this ability to properly sterilize the tissue in the vicinity of the target contributes to the success of radiation treatment (6, 7). The rationale for such sterilization of the tumor periphery is utilized, for example, in radiotherapy intraoperative procedures. The second advantage of dose distributions for irradiations (A2) and (A3) over dose distribution for irradiation (A1) becomes apparent when one realizes that the decrease in dose in the xz plane, i.e. the plane where doses outside the target have highest values at a given distance from the tumor, is faster for (A2) and (A3) beam setups than the speed of dose reduction away from the tumor for (A1) uniform, coplanar irradiation. For example, the ratio of doses for (A1) and (A2) irradiations at a distance from the target of half the tumor radius ($r = 1.5$) is 1.8 (i.e. $D^{xz}_{A1}(1.5)/D_{A2}(1.5) \cong 1.8$) and at a distance from the target equal to one tumor radius ($r = 2$) the ratio is as large as 2.5 (i.e. $D^{xz}_{A1}(2)/D_{A2}(2) \cong 2.5$). Even though the last comparison is useful for illustration of the general principle, it is more interesting from a clinical point of view to compare uniform, coplanar (A1) and clinically feasible, isotropic (A3) irradiation at these characteristic distances. In this comparison the difference is less dramatic; nevertheless, the ratio of doses ($D^{xz}_{A1}(1.5)/D^{xz}_{A3}(1.5)$) and ($D^{xz}_{A1}(2)/D^{xz}_{A3}(2)$) are significantly lager than 1 (they are equal to 1.3 and 1.8, appropriately). In other words, at the distance of one tumor radius from the target boundary the uniform, coplanar (A1) irradiation dose is 80% higher than the dose from the clinically feasible, isotropic (A3) non-coplanar irradiation.

In more general mathematical terms we can quantify this advantage by noticing that for large r (in relation to tumor size, i.e. in relation to $r = 1$) the dose decline in the xz plane for uniform, coplanar irradiation (A1) approximates the $1/r$ function while for isotropic, non-coplanar (A2) irradiation this decline approximates function $1/r^2$. Thus for radioablation, where the speed of dose decline away from the tumor volume (in the plane where doses outside of the target have highest values at a given distance from tumor) is a crucial factor in managing treatment toxicity, the non-coplanarity of the therapy is a highly desirable property of beam arrangements for most effective treatments.

Optimal arrangements of beam directions

Previous discussion has shown the advantage of non-coplanar beam arrangements over coplanar beam arrangements for ESR treatments. The equivalent principle applies for irradiation in which it is not practical to utilize more than a few non-coplanar beams. In these cases, however, it is crucial to define unambiguously what the most isotropic distribution of beam directions (for a given number of beams) really means. Different criteria can be used as the measures of 'isotropicity' when few beams directions are involved (15–17). The most natural criterion from the point of view of the ESR therapy is minimization of the volume outside of the target exposed to the highest dose. This is equivalent to minimizing the volume of intersection of all beams. This problem has been investigated in the past and appropriate algorithms capable of determining optimal distributions of beam directions for a given number of beams have been designed (16, 17). In these earlier papers situations were considered where no restrictions were imposed on the choice of directions of beams. However, generic algorithms designed earlier in (16) can be easily modified to include the appropriate constraints and in this new form they may be utilized to answer questions related to optimal distribution of beam directions for ESR therapy.

First, these algorithms served as a probe for determining the number of beams required for adequate and practical (in the sense of time constraints) ESR treatments. In this evaluation we determined the number of beams that, under generic conditions, provide the most appropriate arrangement for the geometry of dose delivery. To strike a proper balance between a reasonably restricted number of beams and a large enough number of beams (so that dose distributions are not significantly improved as beam number increases further), one needs to investigate multiple sequences of beams' sets. We have found before (16) that increasing the number of beams beyond 7 does not improve dose distributions by more than the value of the potential error of dose calculation algorithms.

Second, following the indication that 7 is the most practical number of beams for ESR therapy using the standard linear accelerator, calculations were done to find their optimal placement relative to patient geometry. These calculations determined beam directions that maximize the dose gradient in all directions. In calculations of 7 most 'isotropic' beam directions, restrictions have been imposed on the range of beam angles relative to the patient to satisfy constraints imposed by equipment (collisions of couch and gantry, etc). This was achieved by the modification of a random search algorithm from (16) by imposing relevant restrictions for the mutual range of rotations for the angle of the gantry (g) and the angle of the couch (c). These restrictions are implemented in the algorithm by relating first pairs of angles (φ, θ) and (c, g) through transformations

$$(i) \quad (c,\ g) = (\varphi,\ \theta)$$

$$(ii) \quad (c, g) = \begin{cases} (\varphi - \pi,\ 2\pi - \theta) & \text{for} \quad \varphi \geq \pi \\ (\varphi + \pi,\ 2\pi - \theta) & \text{for} \quad \varphi < \pi \end{cases} \qquad [1.4]$$

where transformation (i) covers all couch and gantry positions with $g \in [0, \pi)$ and where transformation (ii) covers all couch and gantry positions with $g \in [\pi, 2\pi)$. The next step then requires rejection of these randomly chosen angles (φ, θ) that violate restrictions imposed on parameters (c, g) by the specific dose-delivery equipment (in our case the Siemens KD2 machine with standard couch). These restrictions are shown explicitly in Fig. 3. Thus, if for a given (φ, θ) any of the transformations above (i.e. transformation (i) or transformation (ii)) give a pair (c, g) that belongs to the shaded area of Fig. 3, then this pair (φ, θ) is rejected in the random search optimization algorithm. As a result, pairs (c, g) that minimize the volumes of intersection of all beams around the tumor and are at the same time achievable with standard radiotherapy linear accelerators were found. The set of angle pairs (c, g) providing optimal, or very close to optimal, distribution of beam directions is not unique. This observa-

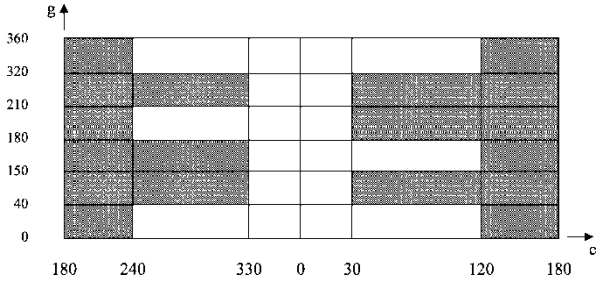

Fig. 3. Domains of gantry g (vertical axis) and couch c (horizontal axis) angles for radiotherapy treatments with linear accelerator. If for a given point $P(\varphi, \theta)$ on the unit sphere S transformations [1.4] give pairs (c, g) of couch and gantry angles that belong to the unshaded area of angular parameters depicted above, then the beam characterized by the central axis passing through the point $P(\varphi, \theta)$ is admissible for stereotactic body frame (SBF) treatments with Siemens KD2 linear accelerator. Otherwise (i.e. when the pair (c, g) of couch and gantry angles belongs to the shaded area of angular parameters above) the central axis passing through the point $P(\varphi, \theta)$ is not admissible for SBF treatments.

tion allows us to look for a solution to the set of 7 beam angles that are the most convenient during treatment and are at the same time optimally distributed. These beam sets that satisfy the conditions of Fig. 3, are displayed in the Table 1. Calculations based on a random search algorithm allow us to determine that the beam sets in the Table 1 lead to volumes of all beam intersections that do not exceed 0.5% of the true minimum volume.

Non-uniform dose distributions

Considerable effort is employed in conventional radiotherapy to create uniform dose distributions in target volumes, including flattening filters, wedges, compensators, and multileaf collimators. Such a dose distribution is desirable assuming the tumor is equally radiosensitive throughout its spatial extension and that its radiosensitivity does not change with time. However, these assumptions are generally not valid. The core of a gross tumor derives its oxygen and nourishment from blood vessels at the periphery. As the tumor grows, the distance from the core to the periphery increases resulting in hypoxia, malnourishment and eventually necrosis. Since hypoxia is associated with resistance to radiation, there exists a gradient of radiosensitivity across the diameter of a tumor. Ideally, one would give a higher dose to the central core to counteract this gradient of sensitivity. Nevertheless, the common practice in radiation therapy is to prescribe uniform dose distributions to target volumes for multifraction (20–30 fractions) radiation therapy despite the existing gradient of sensitivity between the edge and the center of the tumor. That such an approach is clinically effective can be explained by the fact that the process of tumor cell killing during multifraction (20–30 fractions) therapy has a specific dynamics. First, the tumor shrinks during the fractionated therapy and, in turn, the process of substitution of less-resistant cancerous cells at the edge of the target with healthy tissue continues over the time of treatment. Consequently, uniform doses to the whole volume of the originally defined target for multifractionated therapy do, in effect, deliver more of the dose to centrally located, radioresistant, hypoxic cells than to tumor cells that reside initially at the outer edges of the tumor. In contrast, for treatments that use only one fraction (or a small number of fractions, say 2 or 3) the process of tumor cell substitution occurs only after the completion of the treatment. Therefore higher doses delivered to the central portion of the tumor in this fractionation scheme seem equivalent to standard; uniform throughout the target, doses prescribed for fractionated therapy. These higher doses to central tumor regions may be interpreted as a concurrent boost to lesion areas where most resistant cancer cells reside.

Table 1

Parameters provide seven admissible pairs of beam angles (in degrees) for the non-coplanar SBF body radioablation. These directions of beams optimize arrangement of beam positions in angular space (provided constraints shown in by Fig. 3 are satisfied) minimizing the volume of intersection of all cylindrical beams irradiating a spherical tumor

Right side lesion		
$(c, g) = (0, 225)$	$\leftrightarrow$	$(\varphi, \theta) = (180, 135)$
$(c, g) = (0, 315)$	$\leftrightarrow$	$(\varphi, \theta) = (180, 45)$
$(c, g) = (30, 90)$	$\leftrightarrow$	$(\varphi, \theta) = (30, 90)$
$(c, g) = (330, 90)$	$\leftrightarrow$	$(\varphi, \theta) = (330, 90)$
$(c, g) = (90, 40)$	$\leftrightarrow$	$(\varphi, \theta) = (90, 40)$
$(c, g) = (90, 320)$	$\leftrightarrow$	$(\varphi, \theta) = (270, 40)$
$(c, g) = (0, 165)$	$\leftrightarrow$	$(\varphi, \theta) = (0, 165)$
Left side lesion		
$(c, g) = (0, 135)$	$\leftrightarrow$	$(\varphi, \theta) = (0, 135)$
$(c, g) = (0, 45)$	$\leftrightarrow$	$(\varphi, \theta) = (0, 45)$
$(c, g) = (330, 270)$	$\leftrightarrow$	$(\varphi, \theta) = (150, 90)$
$(c, g) = (30, 270)$	$\leftrightarrow$	$(\varphi, \theta) = (210, 90)$
$(c, g) = (90, 40)$	$\leftrightarrow$	$(\varphi, \theta) = (90, 40)$
$(c, g) = (90, 320)$	$\leftrightarrow$	$(\varphi, \theta) = (270, 40)$
$(c, g) = (0, 195)$	$\leftrightarrow$	$(\varphi, \theta) = (180, 165)$

In many cases of ESR, these non-uniform dose distributions develop naturally due to small sizes of beams and ensuing beam disequilibrium at the fields' edges that generally coincide with the edges of tumor volumes. This phenomenon is characteristic for homogeneous as well as non-homogeneous media. In addition, the non-uniform characteristic of dose distribution for small targets is further enhanced if the tumor has a physical density higher than that of the surrounding tissue (e.g. solid tumor in the lung). It is also enhanced when the energy of the beam under consideration increases. In cases when non-uniform dose distributions do not develop naturally, it may be desirable to produce dose distributions that result in the highest dose to be delivered to centrally located radioresistant cells within the target. This can be achieved by appropriately modulating beam intensity with milled compensators or by beam field segmentation with multileaf jaws. In the following section we investigate, in the model situation, the general principle of the interaction between beam profiles and dose distributions when many beams impinging on the patient from different directions are utilized during treatment.

Intensity-modulated beams for non-uniform dose distributions

The results [4.1] and [4.3], can be generalized to cases (A1) of uniform, coplanar and (A2) isotropic, non-coplanar irradiations in which beams with non-uniform intensities over D are utilized. Our interest in these types of irradiation stems from the need for non-uniform shaping of dose distribution within the tumor, which has been discussed in the previous section. Let us recall that to mimic Gamma Knife type dose distributions we need not only a rapid dose decline away from the tumor but also a considerably enhanced dose at the center of the tumor. This dose enhancement can be realized if the intensity of the beams

in coplanar, or non-coplanar, irradiations is increased towards the center of circle D. The typical intensity function P_{par}, satisfying these requirements can, for example, have asymmetric paraboloid shape and be represented by

$$P_{par}(x,\ y) = \begin{cases} -(x^2+y^2)+2 & \text{for} \quad x^2+y^2 \le 1 \\ 0 & \text{for} \quad x^2+y^2 > 1 \end{cases} \qquad [1.5]$$

This expression of the beam intensity profile defines respective fluences at point A at distance r from the origin O as a function of beam direction (φ, θ) in the following manner. For uniform, coplanar irradiation (A1) the above expression for fluence at an arbitrary point A chosen in the xz plane located at a distance r from the origin O has the form

$$f^{A}_{(\varphi,\ \theta)} = \begin{cases} -r^2 \sin^2\varphi + 2 & \text{if} \quad P(\varphi,\ \theta) \in \beta \\ 0 & \text{otherwise} \end{cases} \qquad [1.6]$$

while for isotropic, non-coplanar irradiation this expression for fluence at A at distance r from O (anywhere in space, in particular, also at distance r from O along the y-axis) this fluence can be expressed as

$$f^{A}_{(\varphi',\ \theta')} = \begin{cases} -r^2 \sin^2\phi' + 2 & \text{if} \quad P(\varphi',\ \theta') \in \beta \\ 0 & \text{otherwise} \end{cases} \qquad [1.7]$$

As a result, dose distributions $D^{xz}_{A1par}(r)$ [5.1] and $D_{A\,2par}(r)$ [5.2] can be calculated (see Appendix B for explicit formulas) for coplanar (A1) and isotropically non-coplanar (A2) irradiations, respectively, when paraboloid modulation of beam intensities is applied. Graphs of functions $D^{xz}_{A1par}(r)$ [5.1] and $D_{A\,2par}(r)$ [5.2] are explicitly displayed in Fig. 4. Graphs of these functions demonstrate the combined effect of the beam's profile shaping and multiple addition of beams in the irradiated volume. In particular, it is important to notice that the decrease to half of the maximal value of the intensity function P_{par} from the center of a circle D to its periphery translates into considerably less decrease between the dose to the isocenter and the dose to the periphery of the spherical target S. In the case of coplanar irradiation (A1), the dose at the tumor periphery is about two-thirds of the maximum dose (at isocenter). In the case of non-coplanar, isotropic irradiation (A2), the dose at the tumor periphery is about three-quarters of the maximum dose (at isocenter). The heuristic understanding of this result stems from the realization that the profile of the beam intensity will be translated to the same profile of fluence, and subsequently the dose in the tumor volume, but only in the direction perpendicular to the beam's axis. In contrast, for points in the target that are located along each line that is coincident with the direction of the beam's axis, the fluence, in the first order approximation considered in this paper, remains constant. In consequence, the dose to these points remains constant, too. The difference, when multiple fields are applied, in the fall-off of the dose towards the periphery of the target in comparison with the corresponding fluence fall-off of beam intensities has to be taken into account during the treatment planning process. In particular, this means that the demand of 20% inhomogeneity throughout the tumor volume will necessitate considerably larger (of the order of 40%) variation of intensity throughout the cross-section of each beam utilized during the multiple non-coplanar beam arrangement treatment. These principles have to be taken into account in the construction of beam intensities during the planning process.

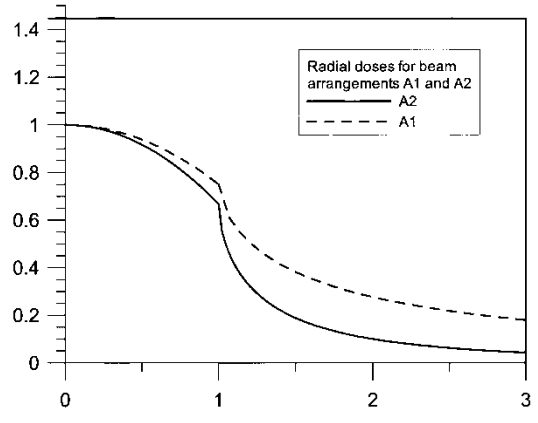

Fig. 4. Dose distributions for irradiations (A1) dashed line, and (A2) continuous line, obtained with beams of paraboloid intensity. The dose distribution for irradiation (A1) has rotational symmetry in the xz plane and is displayed as a function of the distance from the center of the tumor O to any point in this plane. The dose distribution for irradiation (A2) has spherical symmetry and is displayed here as a function of the distance from the center of the tumor O to any point in space.

2. NUMERICAL RESULTS (EXAMPLE CASES)

Generic properties of most select dose distributions for the ESR therapy discussed in this paper may be confronted with numerical, treatment-planning-derived calculations obtained for clinical cases equivalent to the idealized situations of the previous sections.

For instance, in the situation illustrated in Fig. 2a it is easy numerically to calculate with any treatment planning system (Elekta, Render system in our case) the distribution for uniform rotational, co-planar therapy (case (A1)) for clinical beams that include penumbra and attenuation effects. Scoring the doses for this therapy is a routine exercise that gives results, as displayed in Fig. 2b. However, calculating dose distribution for cases (A2) and (A3) is not directly computable with existing planning systems. However, Fig. 2b confirms that the results for an idealized and clinically realistic version of the geometrical arrangement (A1) are equivalent (up to smoothing properties for realistic beams) and thus indicate that general properties, and mutual relations, between cases (A2) and (A3) calculated analytically under geometrically idealized beam shapes are

also valid for beams defined through their clinically realistic versions.

Finally, let us discuss dose distributions for idealized cases of the ESR therapy derived in the previous sections with dose distributions achievable in clinical situations, provided that treatment parameters derived for idealized situations (beam directions, beam intensity shaping, etc.) are applied in the planning of clinical treatments. We make these comparisons for typical ESR lung treatment. One of the most important indicators of the quality of the dose distribution in ESR therapy is the speed with which the dose decreases from the prescribed value at the edge of the tumor (usually 80% of the dose to isocenter) to half of this dose (usually 40% of the dose to isocenter). In other words, it is critical that the volume of the healthy tissue outside of the target that is exposed to dose levels between 80% (Fig. 5a) and 40% (Fig. 5b) of the dose at the isocenter is minimized. Then the portion of the irradiated organ (organs) that has a relatively high probability of being permanently damaged or rendered dysfunctional by ESR treatment is minimized. This dose fall-off for typical ESR treatment case is illustrated by comparison between Figs. 5a, 5b and 5c. Fig. 5c illustrates also the fact that practically achievable dose distributions are still characterized by different gradients along axes x, y and z. Despite our efforts to produce treatments with equal gradients in all directions, the decrease along the y-axis (patient inferior–superior direction) may still be too steep while the decrease along the

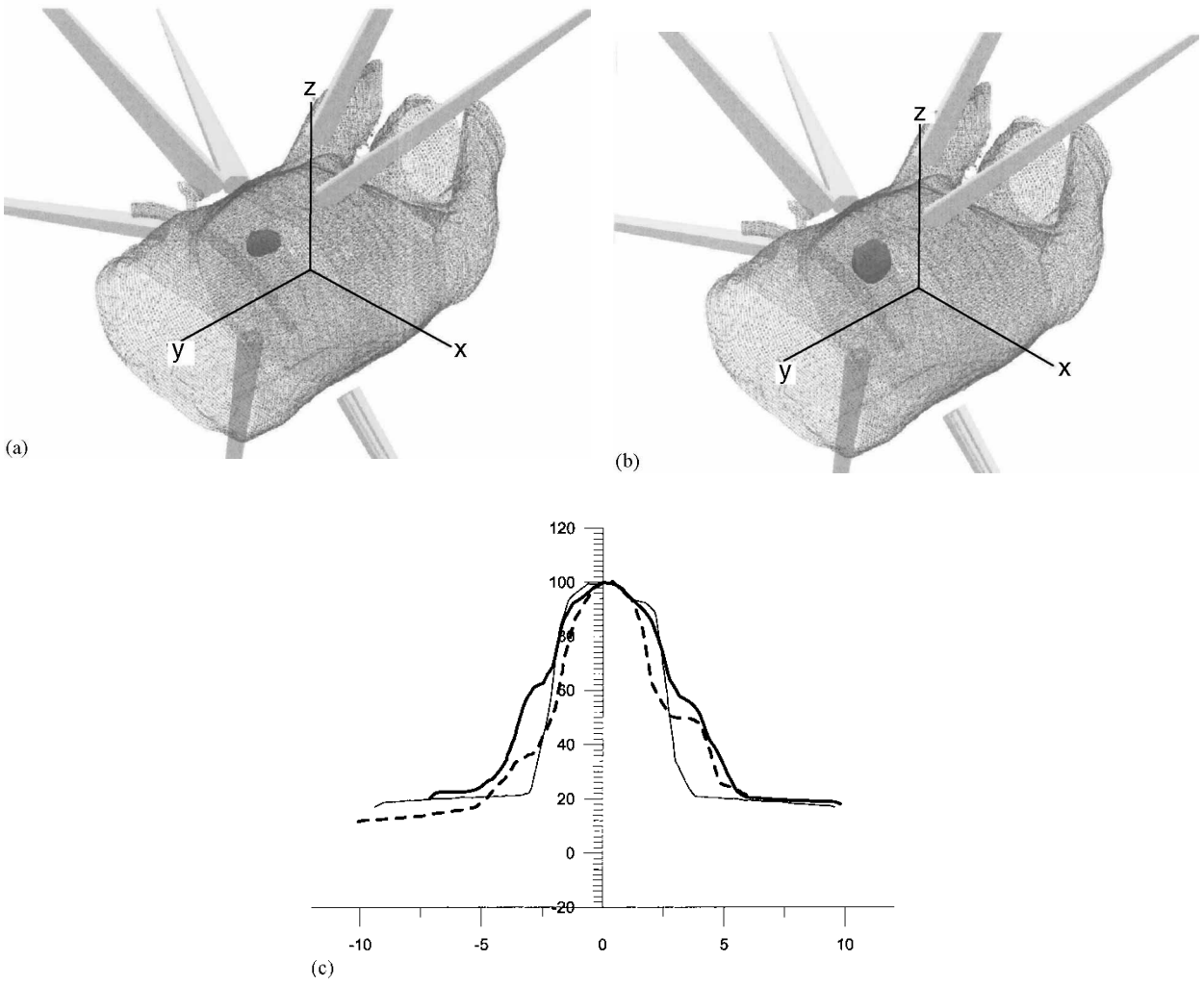

Fig. 5. (a) Distribution of beam directions (Table 1: right lesion) and of the coincidence of the isosurface of 80% dose (prescribed dose) with the outline of the PTV for a typical Render Plan-generated dose distribution for extracranial stereotactic radioablation (ESR) treatment with parabolically modulated intensities of beams. (b) Distribution of beam directions (Table 1: right lesion) and the volume of tissue exposed to the dose (40%+, i.e. larger than half of the dose prescribed) for a typical Render Plan-generated dose distribution for ESR treatment with parabolically modulated intensities of beams. (c) Variation of dose distribution along the x, y- and z-axes for a typical Render Plan-generated dose distribution for ESR treatment (the same as in (a) and (b)) with optimized distribution of beam directions (Table 1: right lesion) and parabolically modulated intensities of beams. — Profile along z axis, — Profile along y axis, – – – Profile along x axis.

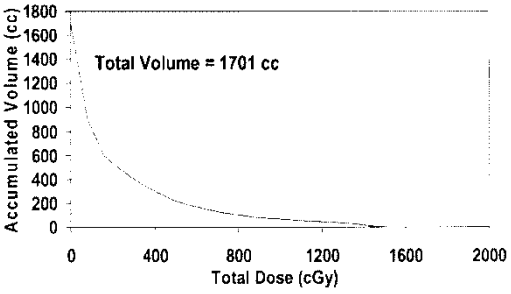

Fig. 6. Integral DVH for the treatment of the lung depicted in Figs. 5a, 5b and 5c.

z-axis (patient anterior–posterior direction) may still be too slow for optimal treatment. These differences result from irregular geometry of the patient's body, non-central positioning of the target and also from the limited number of beams utilized during the treatment.

Another important indicator of the quality of dose distribution in ESR therapy, especially in cases when the target is completely embodied within a particular organ, is the DVH of this organ. For example, in Figs. 5a, 5b and 5c (for which the tumor is fully contained in the lung) the DVH of the lung is presented in Fig. 6. The histogram in Fig. 6 illustrates that the volume of high dose around the tumor constitutes only a small portion of the organ itself. In the particular example illustrated, only 12% (200 cc) of the total lung volume (1700 cc) is exposed to more than half of the dose prescribed to the tumor periphery. Thus Figs. 5a, 5b and 5c and Fig. 6 illustrate jointly that the dose distributions we achieve in the approach to ESR therapy using the techniques described in this paper, despite all their irregularities, are capable of closely irritating close distribution of Gamma Knife treatments of brain lesions.

3. CONCLUSIONS

The appropriate implementation of the ESR technique amounts to a radical change in treatment routines compared to conventional radiotherapy. In particular, these techniques require considerable alteration of dose distribution shaping and dose delivery compared with traditional radiotherapy techniques. These alterations of dose distributions together with their justification have been analyzed in the paper. In brief, we have shown that using linear accelerators as a source of photons, tumors located in the chest or the abdomen can be irradiated during ESR therapies in a fashion imitating treatments of intracranial targets with Gamma Knife. We have shown in particular that by using linear accelerators as a source of photons, the following conditions of dose distributions that are necessary for properly executed ESR treatments can be achieved: 1) shaping the prescription iso-surface so that it coincides with the outline of the target in such a way that the highest doses delivered outside of the tumor are confined to regions that spread uniformly on the outer boundary of the targeted volume, 2) creating rapid fall-off of dose from the tumor volume to healthy tissue isotropically in all directions and 3) generating non-uniform dose distribution throughout the volume of the tumor, with the highest dose delivered to the central portion of the tumor where hypoxic cells potentially reside.

4. APPENDIX A

For cases (A1), (A2) and (A3) of irradiation considered in this paper, weights w_i are equal for all beams involved (see discussion in Section 1). Therefore, measure μ representing these weights, are uniformly spread over the circle K for coplanar irradiation (A1), over the whole sphere S for isotropic, non-coplanar irradiation (A2) and over the subset PS 2.2 of sphere S for clinically feasible, isotropic non-coplanar irradiation (A3), respectively. Thus, in mathematical terms these measures are equivalent to the length of the arc (defined by $\mu(dP(\varphi,\ \theta)) = d\theta/\pi$), for (A1) irradiation, and to the area of the surface of the unit sphere (defined by $\mu(dP(\varphi,\ \theta)) = (1/4\pi)\sin\theta\ d\theta\ d\varphi$) for non-coplanar irradiations (A2) and (A3). Consequently, the normalized dose $D^{xz}_{A1}(r)$ to point A at distance r from O on axial plane xz for coplanar irradiation (A1) can be evaluated (in the first order approximation defined in Section 1) as

$$D^{xz}_{A1}(r) = \frac{1}{\pi}\int \chi^A_\beta(\varphi,\ \theta)\ d\theta = \frac{1}{\pi}\int_\beta d\theta$$

$$= \begin{cases} \dfrac{1}{\pi}\displaystyle\int_0^{\pi} d\theta & \text{for } r<1 \\ 2\dfrac{1}{\pi}\displaystyle\int_0^{\arcsin(1/r)} d\theta & \text{for } r\geq 1 \end{cases}$$

$$= \begin{cases} 1 & \text{for } r<1 \\ \dfrac{2}{\pi}\arcsin\dfrac{1}{r} & \text{for } r\geq 1 \end{cases} \qquad [4.1]$$

and the dose $D^{y}_{A1}(r)$ to point A at distance r from O along the y-axis (perpendicular to axial xz plane and crossing origin O) as

$$D^{y}_{A1}(r) = \frac{1}{\pi}\int \chi^A_\beta(\varphi,\ \theta)\ d\theta = \frac{1}{\pi}\int_\beta d\theta$$

$$= \begin{cases} 1 & \text{for } r<1 \\ 0 & \text{for } r\geq 1 \end{cases} \qquad [4.2]$$

Furthermore, the normalized dose $D_{A2}(r)$ to point A along any radial direction at distance r from O for isotropic, non-coplanar irradiation (A2) can be evaluated as

$$D_{A2}(r)=\frac{1}{4\pi}\int \chi_{\beta}^{A}(\varphi,\ \theta)\sin\,\theta\,d\theta\,d\varphi=\frac{1}{4\pi}\int_{\beta}\sin\,\theta\,d\theta\,d\varphi$$

$$=\begin{cases}\dfrac{1}{2\pi}\displaystyle\int_0^{\pi}\sin\,\theta\,d\theta\int_0^{2\pi}d\varphi & \text{for } r<1\\ \dfrac{1}{2\pi}\displaystyle\int_0^{\arcsin(1/r)}\sin\,\theta\,d\theta\int_0^{2\pi}d\varphi & \text{for } r\geq 1\end{cases}$$

$$=\begin{cases}1 & \text{for } r<1\\ \dfrac{r-\sqrt{(r^2-1)}}{r} & \text{for } r\geq 1\end{cases} \qquad [4.3]$$

Finally, for clinically feasible., non-coplanar irradiation (A3) dose $D_{A3}^{xz}(r)$ to point, A at distance r from O on axial plane xz is given as

$$D_{A3}^{xz}(r)=\frac{1}{4\pi}\int \chi_{\beta}^{A}\,(\varphi,\ \theta)\,\sin\,\theta\,d\theta\,d\varphi=\frac{1}{4\pi}\int_{\beta}\sin\,\theta\,d\theta\,d\varphi$$

$$=\begin{cases}\sqrt{2}-1+\dfrac{4}{\pi\sqrt{2}}\displaystyle\int_{\pi/4}^{\arcsin 1}\arcsin\left(\frac{\sqrt{2}}{2\,\sin\,\theta}\right)\sin\,\theta\,d\theta & \text{for } r<1\\ \sqrt{2}-1+\dfrac{4}{\pi\sqrt{2}}\displaystyle\int_{\pi/4}^{\arcsin(1/r)}\arcsin\left(\frac{\sqrt{2}}{2\,\sin\,\theta}\right)\sin\,\theta\,d\theta & \text{for } 1\leq r<\sqrt{2}\\ \dfrac{1}{\pi\sqrt{2}}\displaystyle\int_0^{\arcsin(1/r)}\sin\,\theta\,d\theta\int_0^{2\pi}d\varphi & \text{for } \sqrt{2}\leq r\end{cases}$$

$$=\begin{cases}1 & \text{for } r<1\\ \sqrt{2}-1+\dfrac{4}{\pi\sqrt{2}}\displaystyle\int_{\pi/4}^{\arcsin(1/r)}\arcsin\left(\frac{\sqrt{2}}{2\sin\,\theta}\right)\sin\,\theta\,d\theta & \text{for } 1\leq r<\sqrt{2}\\ \sqrt{2}\dfrac{r-\sqrt{(r^2-1)}}{r} & \text{for } \sqrt{2}\leq r\end{cases} \qquad [4.4]$$

and dose $D_{A3}^{y}(r)$ to point A at distance r from O along the y-axis (perpendicular to axial xz plane and crossing origin O) is equal to

$$D_{A3}^{y}(r)=\frac{1}{4\pi}\int \chi_{\beta}^{A}(\varphi,\ \theta)\sin\,\theta\,d\theta\,d\varphi=\frac{1}{4\pi}\int_{\beta}\sin\,\theta\,d\theta\,d\varphi$$

$$=\begin{cases}1 & \text{for } r<1\\ \dfrac{2}{\sqrt{2}}\dfrac{1}{2\pi}\displaystyle\int_{\pi/4}^{\arcsin(1/r)}\sin\,\theta\,d\theta\int_0^{2\pi}d\varphi=1-\sqrt{2}\sqrt{\frac{r^2-1}{r}} & \text{for } 1\leq r<\sqrt{2}\\ 0 & \text{for } \sqrt{2}\leq r\end{cases} \qquad [4.5]$$

5. APPENDIX B

The formula 2.6 leads to the following expression for the normalized expression dose $D^{xz}_{A1par}(A)$ to point A (at distance r from O in plane xy) for uniform, coplanar irradiation with paraboloidal-shaped intensity beams

$$
\begin{aligned}
D^{xz}_{A1par}(r) &= \frac{1}{4\pi}\int_{\beta}(-r^2\sin^2\varphi+2)\,d\varphi \\
&= \begin{cases} \dfrac{1}{\pi}\displaystyle\int_0^{2\pi}(-r^2\sin^2\varphi+2)\,d\varphi & \text{for } r<1 \\ 4\dfrac{1}{4\pi}\displaystyle\int_0^{\arcsin(1/r)}(-r^2\sin^2\varphi+2)\,d\varphi & \text{for } r\geq 1 \end{cases} \\
&= \begin{cases} -\dfrac{1}{4}r^2+1 & \text{for } r<1 \\ \dfrac{1}{\pi}\left(\dfrac{1}{2}\,r\sqrt{\left(\dfrac{r^2-1}{r^2}\right)}-\dfrac{1}{2}\,r^2\arcsin\dfrac{1}{r}+2\arcsin\dfrac{1}{r}\right) & \text{for } r\geq 1 \end{cases}
\end{aligned}
\qquad [5.1]
$$

Analogously, the formula [1.7] leads to the expression for normalized dose $D_{A\,2par}(r)$ to point A (at distance r from O anywhere in space) for isotropic, non-coplanar irradiation with paraboloidal-shaped intensity beams

$$
\begin{aligned}
D_{A2par}(r) &= \frac{1}{8\pi}\int\chi^A_\beta(\varphi,\ \theta)\sin\theta\,d\theta\,d\varphi = \frac{1}{8\pi}\int_{\beta}(-r^2\sin^2\theta+2)\sin\theta\,d\theta\,d\varphi \\
&= \begin{cases} \dfrac{1}{8\pi}\displaystyle\int_0^{\pi}(-r^2\sin^2\theta+2)\sin\theta\,d\theta\int_0^{2\pi}d\varphi & \text{for } r<1 \\ \dfrac{1}{4\pi}\displaystyle\int_0^{\arcsin(1/r)}(-r^2\sin^2\theta+2)\sin\theta\,d\theta\int_0^{2\pi}d\varphi & \text{for } r\geq 1 \end{cases} \\
&= \begin{cases} 1-\dfrac{1}{3}\,r^2 & \text{for } r<1 \\ -\dfrac{5}{6}\sqrt{\left(\dfrac{r^2-1}{r^2}\right)}+\dfrac{1}{3}\,r^2\sqrt{\left(\dfrac{r^2-1}{r^2}\right)}-\dfrac{1}{3}\,r^2+1 & \text{for } r\geq 1 \end{cases}
\end{aligned}
\qquad [5.2]
$$

REFERENCES

1. Lax I, Blomgren H, Naslund I, et al. Stereotactic radiotherapy of malignancies in the abdomen, Methodological aspects. Acta Oncol 1994; 33: 677–83.
2. Blomgren H, Lax I, Naslund I, et al. Stereotactic high dose fraction radiation therapy of extracranial tumors using an accelerator, Clinical experience of the first thirty-one patients. Acta Oncol 1995; 35: 861–70.
3. Lax L. Target dose versus extratarget dose in stereotactic radiosurgery. Acta Oncol 1993; 32: 453–7.
4. Murphy M, Adler J, Bodduluri M, et al. Image-guided radiosurgery for the spine and pancreas. Comput Aided Surg 2000; 5: 278–88.
5. Hamilton A, Lulu B, Fosmire H, et al. LINAC-based spinal stereotactic radiosurgery. Stereotact Funct Neurosurg 1996; 66: 1–9.
6. Timmerman R, Papiez L, McGarry, et al. Extracranial stereotactic radioablation: results of a phase I study in medically inoperable stage I non-small cell lung cancer patients. Chest 2003: (in press).

7. Timmerman R, Papiez L, Suntharalingam M. Extracranial stereotactic radiation delivery: expansion of technology beyond the brain. TCRT 2003; 2: 153–60.
8. Papiez L. On the equivalence of rotational and concentric therapy. Phys Med Biol 2000; 45: 390–409.
9. Cormack AM. A problem in rotational therapies with x-rays. Int J Radiat Oncol Biol Phys 1987; 13: 623–30.
10. Brahme A, Roos J, Lax I. Solution of an integral equation encountered in rotation therapy. Phys Med Biol 1982; 27: 1220–31.
11. Papiez L, Ringor M. Implications of the reconstruction formula for rotational therapy in treatment planning optimization. Inverse Problems 1997; 13: 1519–32.
12. Ringor M, Papiez L. Inverse planning and optimization: a comparison of solutions. Radiat Phys Chem 1998; 53: 263–74.
13. Oelfke U, Bortfeld T. Inverse planning for x-ray rotation therapy: a general solution of the inverse problem. Phys Med Biol 1999; 44: 1089–104.
14. Giraud A, Antoine M, Larrouy A, et al. Evaluation of microscopic tumor extension in non-small-cell lung cancer for three-dimensional conformal radiotherapy planning. Int J Radiat Oncol Biol Phys 2000; 48: 1015–24.
15. Sailer S, Rosenman L, Symon J, et al. The tetrad and the hexad: maximum beam separation as a starting point for noncoplanar 3D treatment planning: prostate cancer as a test case. Int J Radiat Oncol Biol Phys 1994; 30: 623–30.
16. Papiez L, Lu X, Langer M. On the isotropic distribution of beam directions. Math Mod Meth Appl Sci 2000; 10: 991–1000.
17. Webb S. The problem of isotropically orienting N converging vectors in space with applications to radiotherapy planning. Phys Med Biol 1995; 40: 945–54.